High-Temperature Synthesis of Stable Ordered Mesoporous Silica Materials by Using Fluorocarbon–Hydrocarbon Surfactant Mixtures

Defeng Li, Yu Han, Jiangwei Song, Lan Zhao, Xianzhu Xu, Yan Di, and Feng-Shou Xiao*[a]

Abstract: Highly ordered hexagonal mesoporous silica materials (**JLU-20**) with uniform pore sizes have been successfully synthesized at high temperature (150–220 °C) by using fluorocarbon–hydrocarbon surfactant mixtures. The fluorocarbon–hydrocarbon surfactant mixtures combine the advantages of both stable fluorocarbon surfactants and ordered hydrocarbon surfactants, giving ordered and stable mixed micelles at high temperature (150–220 °C). Mesoporous **JLU-20** shows extraordinary stability towards hydrothermal treatment (100 % steam at 800 °C for 2 h or boiling water for 80 h), thermal treatment (calcination at 1000 °C for 4 h), and toward mechanical treatment (compressed at 740 MPa). Transmission electron microscopy images of **JLU-20** show well-ordered hexagonal arrays of mesopores with one-dimensional (1D) channels and further confirm that **JLU-20** has a two-dimensional (2D) hexagonal (P6*mm*) mesostructure. ^{29}Si HR MAS NMR spectra of as-synthesized **JLU-20** shows that **JLU-20** is primarily made up of fully condensed Q^4 silica units ($\delta = -112$ ppm) with a small contribution from incompletely cross-linked Q^3 ($\delta = -102$ ppm) as deduced from the very high Q^4/Q^3 ratio of 6.5, indicating that the mesoporous walls of **JLU-20** are fully condensed. Such unique structural features should be directly attributed to the high-temperature synthesis, which is responsible for the observed high thermal, hydrothermal, and mechanical stability of the mesoporous silica materials with well-ordered hexagonal symmetry. Furthermore, the concept of "high-temperature synthesis" is successfully extended to the preparation of three-dimensional (3D) cubic mesoporous silica materials by the assistance of a fluorocarbon surfactant as a co-template. The obtained material, designated **JLU-21**, has a well-ordered cubic *Im*3*m* mesostructure with fully condensed pore walls and shows unusually high hydrothermal stability, as compared with conventional cubic mesoporous silica materials such as **SBA-16**.

Keywords: high-temperature synthesis · hydrothermal stability · mechanical stability · mesoporous materials · surfactants

Introduction

The production of mesoporous materials with higher hydrothermal, thermal, and mechanical stability is currently of great interest because these properties are required for potential applications in several fields.[1,2] Recently, a number of mesoporous materials with good hydrothermal stability have been synthesized,[1–10] such as mesoporous MCM-41 with thicker and more highly condensed pore walls synthesized by increasing crystallization time,[3] an ordered hexagonal **SBA-15** with thicker pore walls synthesized in strongly acidic media ($pH < 0$),[4] vesicle-like MSU-G materials with high SiO_4 cross-linking synthesized by using neutral gemini surfactants as the templates,[5] disordered KIT-1 synthesized by using inorganic salts as additives,[6] and stable mesoporous aluminosilicates from a grafting route,[7] from a zeolite seed solution,[8] or preformed zeolite nanoclusters.[9,10] Notably, these mesostructured materials are prepared at room temperature or relatively low temperatures (80–150 °C). This is quite different from the higher temperatures (150–220 °C) used for the synthesis of many microporous crystals of zeolites or phosphates. The reason for this is that surfactant molecules will not be able to direct mesoporous structure formation due to unfavorable conditions for micelle formation at the higher temperatures.[11,12] In some cases, the long-chain surfactants will even decompose at more than 150 °C.

As with silica-based mesoporous materials, a critical factor in increasing stability is to have more silica condensation on the pore walls.[5,7] Low synthesis temperatures result in imperfectly condensed mesoporous walls with large amounts of terminal hydroxy groups that make the mesostructure unstable, especially under hydrothermal conditions

[a] D. Li, Dr. Y. Han, J. Song, L. Zhao, Dr. X. Xu, Y. Di, Prof. F.-S. Xiao
Department of Chemistry & State Key Laboratory of Inorganic Synthesis and Preparative Chemistry
Jilin University, Changchun 130023 (China)
Fax: (+86) 431-516-8624
E-mail: fsxiao@mail.jlu.edu.cn

 DOI: 10.1002/chem.200400188

or on exposure to steam. Reduction of the defects and improvement of the degree of silica condensation in the mesoporous walls is a challenge.

It can be expected that the level of silica condensation will be enhanced by increasing the crystallization temperature.[3] As suggested above, the strategy of using higher crystallization temperatures for the synthesis of mesoporous materials may require special surfactants that can be used as template at such high temperatures. Fluorocarbon surfactants are stable and widely used at high temperatures (>200 °C). However, due to the rigidity and strong hydrophobicity of the fluorocarbon chains,[13] fluorocarbon surfactants are not suitable as templates for the preparation of well-ordered mesoporous materials.

On the other hand, it has been reported that fluorocarbon surfactants are easy to mix with other surfactants to form surfactant mixtures.[14] Surfactant mixtures could therefore possibly combine the advantages of both hydrocarbon surfactant (ordered micelle) and fluorocarbon surfactant (stable micelle at higher temperature, 150–220 °C).

In our preliminary work, we have briefly reported on the synthesis of the ordered mesoporous silica material **JLU-20**, which was synthesized at higher temperature (150–220 °C) by using fluorocarbon–hydrocarbon surfactant mixtures (**FC-4** with **P123**).[15] We report herein details of the synthesis, structure, characterization, and excellent thermal, hydrothermal, and mechanical stability of **JLU-20**. Furthermore, when the fluorocarbon surfactant **FC-4** is mixed with **F127** ($EO_{106}PO_{70}EO_{106}$) and this mixture is used as the template, highly ordered cubic mesoporous silica materials with unusual hydrothermal stability, designated **JLU-21**, are successfully synthesized at high temperatures (140–200 °C).

Results and Discussion

Ordered hexagonal silica materials (JLU-20)

X-ray diffraction (XRD): The XRD pattern of as-synthesized **JLU-20** (Figure 1A-a) exhibits three obvious peaks assigned to a hexagonal symmetry. The intense (100) peak reflects a *d* spacing of 101 Å, corresponding to a large unit cell parameter ($a = 118$ Å). After calcination at 650 °C, **JLU-20** (Figure 1A-b) clearly shows four well-resolved peaks that can be indexed as the (100), (110), (200), and (210) diffractions associated with the *p6mm* hexagonal symmetry with a lattice constant $a = 118$ Å. Notably, as-synthesized and calcined **JLU-20** has the same unit cell constant (118 Å), indicating that the unit cell of **JLU-20** does not contract during calcination at 650 °C for 5 h. In addition, the calcined **JLU-20** (Figure 1A-b) exhibits a strong peak associated with the (200) reflection, whereas the peak assigned to the (110) reflection is relatively weaker. This result suggests that the cal-

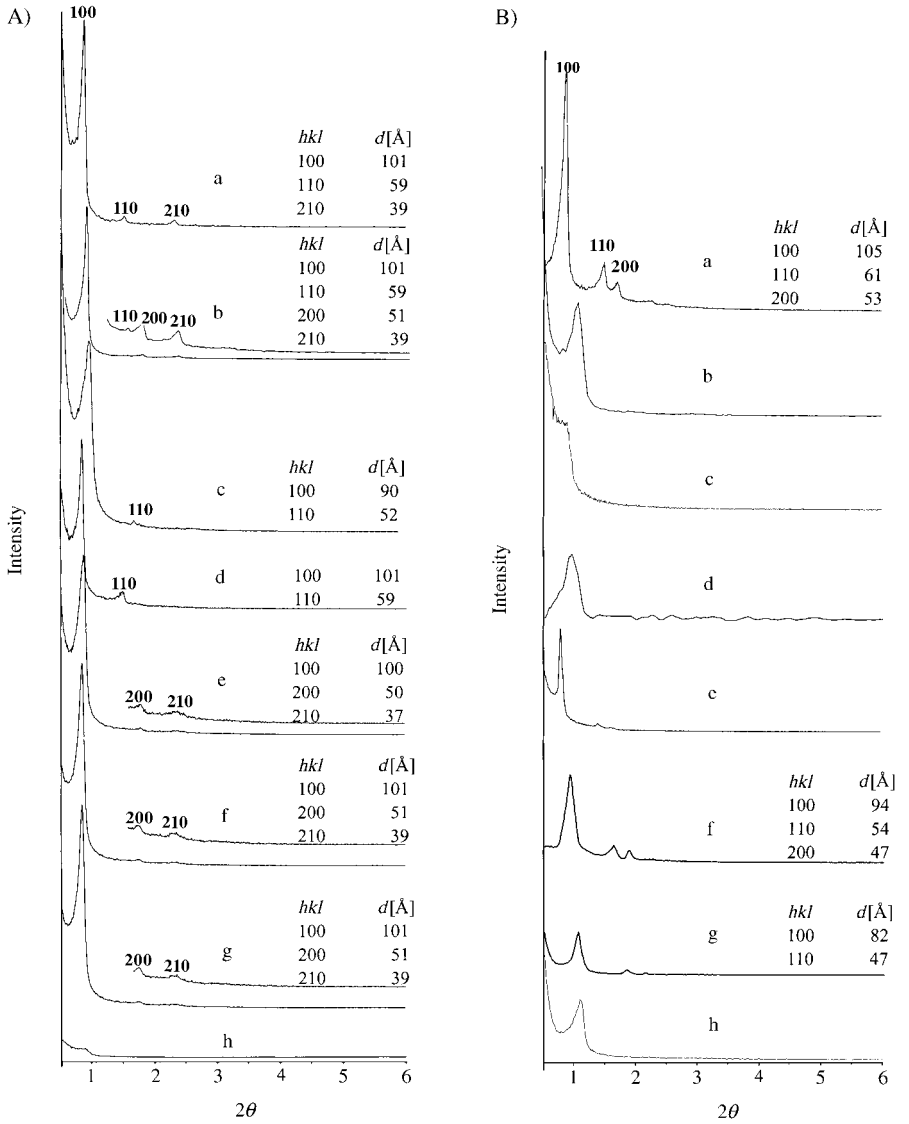

Figure 1. A) XRD patterns of as-synthesized **JLU-20** (a), **JLU-20** calcined at 650 °C (b), **JLU-20** calcined at 1000 °C (c), **JLU-20** treated in boiling water for 80 h (d), **JLU-20** treated with 100 % steam at 800 °C for 2 h (e), **JLU-20** compressed at 300 MPa for 10 min (f), **JLU-20** compressed at 740 MPa for 10 min (g), and the sample **SBA-15**(190) synthesized at 190 °C in the absence of **FC-4** (h). B) XRD patterns of **SBA-15** calcined at 500 °C (a), **SBA-15** calcined at 1000 °C (b), **SBA-15** treated in boiling water for 80 h (c), **SBA-15** treated with 100 % steam at 800 °C for 2 h (d), **SBA-15** compressed at 300 MPa for 10 min (e), **SBA-15**(B) calcined at 500 °C (f), **SBA-15** (B) compressed at 300 MPa for 10 min (g), and **SBA-15** (B) compressed at 740 MPa for 10 min (h).

cined **JLU-20** has thicker pore walls than conventional mesoporous materials, because the pore wall thickness (relative to the unit-cell size) tends to increase with an increase in the relative intensity of the (200) peak compared to the (110) peak.[16–19] When **JLU-20** is further calcined at 1000 °C for 4 h, the sample basically still shows its peaks associated with a hexagonal mesostructure, as shown in Figure 1A-c. The first diffraction peak at 0.87° in as-synthesized **JLU-20** is shifted to 0.99° in the sample calcined at 1000 °C due to shrinkage. As a result, the value of the cell lattice parameter, *a*, is shifted from 118 Å to 104 Å. In comparison, after the calcination at 1000 °C for 4 h, **SBA-15** only shows a broad peak assigned to the (100) reflection, and the peaks assigned to the (110) and (200) reflections have completely disappeared (Figure 1B-b), which suggests partial destruction of the hexagonal mesostructure of **SBA-15**. These results indicate that **JLU-20** has much better thermal stability than **SBA-15**.

After treatment of the calcined sample in boiling water for more than 80 h, **JLU-20** shows two clear peaks assigned to the (100) and (110) reflections of the hexagonally ordered mesostructure (Figure 1A-d). In contrast, the treated **SBA-15** shows only a weak peak assigned to the (100) reflection of the mesostructure (Figure 1B-c). After treatment in 100 % steam at 800 °C for 2 h (Figure 1A-e), **JLU-20** shows three obvious peaks associated with the (100), (200), and (210) diffractions of the hexagonal mesostructure. In contrast, the treated **SBA-15** exhibits a very broad peak assigned to the (100) reflection (Figure 1B-d). These results indicate that **JLU-20** has remarkable hydrothermal stability even at high temperatures.

Moreover, when calcined **JLU-20** is compressed at 300 MPa, the sample shows almost the same XRD diffractogram (Figure 1A-f) as the calcined sample (Figure 1A-b); when the pressure is increased to 740 MPa, calcined **JLU-20** still exhibits its typical peaks associated with a hexagonal mesostructure (Figure 1A-g). In contrast, after compression at 300 MPa, **SBA-15** still shows three peaks associated with a hexagonal mesostructure, but their intensities decreased significantly (Figure 1B-e). It has been reported that the mechanical stability is strongly related to the wall thickness of mesoporous materials.[20] Generally, the wall of **JLU-20** (5.5 nm, Table 1) is thicker than that of **SBA-15** (4.3 nm, Table 1). To avoid the effect of the wall thickness, **SBA-15**(B) with thicker walls (6.0 nm, Table 1) was synthesized according to the method reported in reference [21]. After compression at 300 MPa, **SBA-15**(B) also exhibits three peaks typical of a hexagonal mesostruture, but their peak intensities are also reduced (Figure 1B-g). Further increasing the pressure to 740 MPa, **SBA-15**(B) shows only one peak associated with the mesostructure, indicating the partial destruction of its mesostructure (Figure 1B-h). Apparently, **SBA-15**(B) with thicker walls still shows much lower mechanical stability than **JLU-20**. The extraordinary mechanical stability of **JLU-20** should be assigned to the unique route for the synthesis of mesoporous materials at high temperature (150–220 °C), rather than other reasons.

Figure 1A-h shows the XRD pattern of the sample synthesized at 180 °C using a polymeric surfactant (**P123**) in the absence of fluorocarbon surfactant (**FC-4**); only a very weak peak is observed near 0.9°. This result indicates that the ordered sample cannot be synthesized at higher temperature in the absence of the fluorocarbon surfactant. Therefore, we propose that **FC-4** is necessary for the high-temperature synthesis of ordered mesoporous materials.

Table 1. Properties of the samples before and after treatment.[a]

Sample	*d*(100) [Å]	Pore size [Å]	Wall thickness [Å]	Pore volume [$cm^3 g^{-1}$][d]	Surface area [$m^2 g^{-1}$]	Q^4/Q^3+Q^2	*wS/V*
JLU-20	101					6.5	
calcined	101	62	55	0.46	300		4.0
treated[b]	101	66	51	0.44	278		4.2
treated[c]	95	65	45	0.32	225		4.5
1000 °C	90	42	48	0.32	225		
300 MPa	101	63	54	0.46	276		
740 MPa	101	63	54	0.45	246		
SBA-15	110					1.9	
calcined	105	78	43	1.45	1005		5.4
treated [b]				1.03	320		
treated [c]				0.35	214		
1000 °C				0.43	110		
300 MPa				0.46	272		
SBA-15(B)	100						
calcined	94	48	60	1.15	920		
300 MPa	82	37	58	0.45	677		
740 MPa	79	58	57	0.39	559		
SBA-15(190)	99	80		0.34	235		
SFC-4(100)		25		0.34	563		
SFC-4(190)				0.21	256		
JLU-20(100)	108	79	46	1.51	1100		

[a] Pore-size distributions and pore volumes determined from N_2 adsorption isotherms at 77 K and the wall thickness was calculated as: thickness = *a*-pore size ($a = 2 \times d_{(100)}/3^{1/2}$); In the last column, *w*, *S*, and *V* denote pore size, surface area, and pore volume, respectively. [b] Treated in boiling water for 80 h. [c] Treated with 100 % water vapour at 800 °C for 2 h. [d] The pore volume here is the primary mesopore volume (BJH adsorption cumulative pore volume of pores between 20 and 250 Å diameter).

N_2 Isotherms: Figure 2A-a shows the N_2 adsorption–desorption isotherm of **JLU-20** calcined at 650 °C for 5 h, which gives a IV-type isotherm assigned to a 2D hexagonal (*P6mm*) mesostructure. The N_2 adsorption isotherm gives a BET surface area of 300 $m^2 g^{-1}$ and a pore volume of 0.46 $cm^3 g^{-1}$. The pore-size distribution, calculated from the adsorption curve using the BJH model, shows an average pore size of about 6.2 nm (Table 1). When as-synthesized **JLU-20** is calcined at 1000 °C for 4 h, the sample still exhibits a IV-type isotherm, indicating the preservation of the ordered mesostructure (Figure 2A-b). However, the pore size is smaller (4.2 nm), and there is a decrease in surface area of 25 % (from 300 $m^2 g^{-1}$ to 225 $m^2 g^{-1}$, Table 1). In comparison, the same treatment of **SBA-15** (Figure 2B-b) results in a significant decrease in BET surface area of 90 % (from 1005 $m^2 g^{-1}$ to 110 $m^2 g^{-1}$, Table 1) and in pore volume of 70 % (from 1.45 $cm^3 g^{-1}$ to 0.43 $cm^3 g^{-1}$, Table 1). In addition, the treated **SBA-15** shows a poor isotherm (Figure 2B-b). These results confirm that **JLU-20** has much higher thermal stability than **SBA-15**.

After hydrothermal treatment in boiling water for 80 h, **JLU-20** still exhibits a type IV isotherm (Figure 2A-c). The BET surface area and primary mesopore volume of **JLU-20** was reduced by only 7 % from 300 $m^2 g^{-1}$ to 278 $m^2 g^{-1}$ (Table 1) and by only 5 % from 0.46 $cm^3 g^{-1}$ to 0.44 $cm^3 g^{-1}$ (Table 1), respectively, implying good maintenance of the uniform mesostructure. In contrast, **SBA-15** treated under the same conditions shows a poor isotherm (Figure 2B-c). There is a decrease in the BET surface area of 68 % from 1005 $m^2 g^{-1}$ to 320 $m^2 g^{-1}$ (Table 1) and in primary mesopore volume by 30 %, from 1.45 $cm^3 g^{-1}$ to 1.03 $m^2 g^{-1}$ (Table 1). These results also indicate that **JLU-20** has remarkably hydrothermal stability compared with **SBA-15**.

After being kept under a pressure of 300 MPa for 10 min, calcined **JLU-20** shows a characteristic N_2 isotherm associated with hexagonal mesostructures (Figure 2A-d), giving a surface area of 276 $m^2 g^{-1}$, a pore volume of 0.46 $cm^3 g^{-1}$, and an average pore size distribution of 6.3 nm (Table 1). These values are very similar to those of **JLU-20** calcined at 650 °C. When the pressure is increased to 740 MPa, calcined **JLU-20** also shows a N_2 adsorption–desorption isotherm attributed to a hexagonal mesostructure (Figure 2A-e). The surface area is reduced by 18 % from 300 $m^2 g^{-1}$ (in **JLU-20** calcined at 650 °C) to 246 $m^2 g^{-1}$ in **JLU-20** compressed by 740 MPa, but the pore volume or pore-size distribution does not change(Table 1); that is, the surface area of 82 % and pore volume of 98 % remains for **JLU-20** compressed by the pressure of 740 MPa. In contrast, under a pressure of 300 MPa, **SBA-15** shows a very poor N_2 isotherm (Figure 2B-d), accompanied by a decrease in BET surface area of 73 % from 1005 $m^2 g^{-1}$ to 272 $m^2 g^{-1}$ and a decrease in pore volume of 68 % from 1.45 $cm^3 g^{-1}$ to 0.46 $cm^3 g^{-1}$. It is

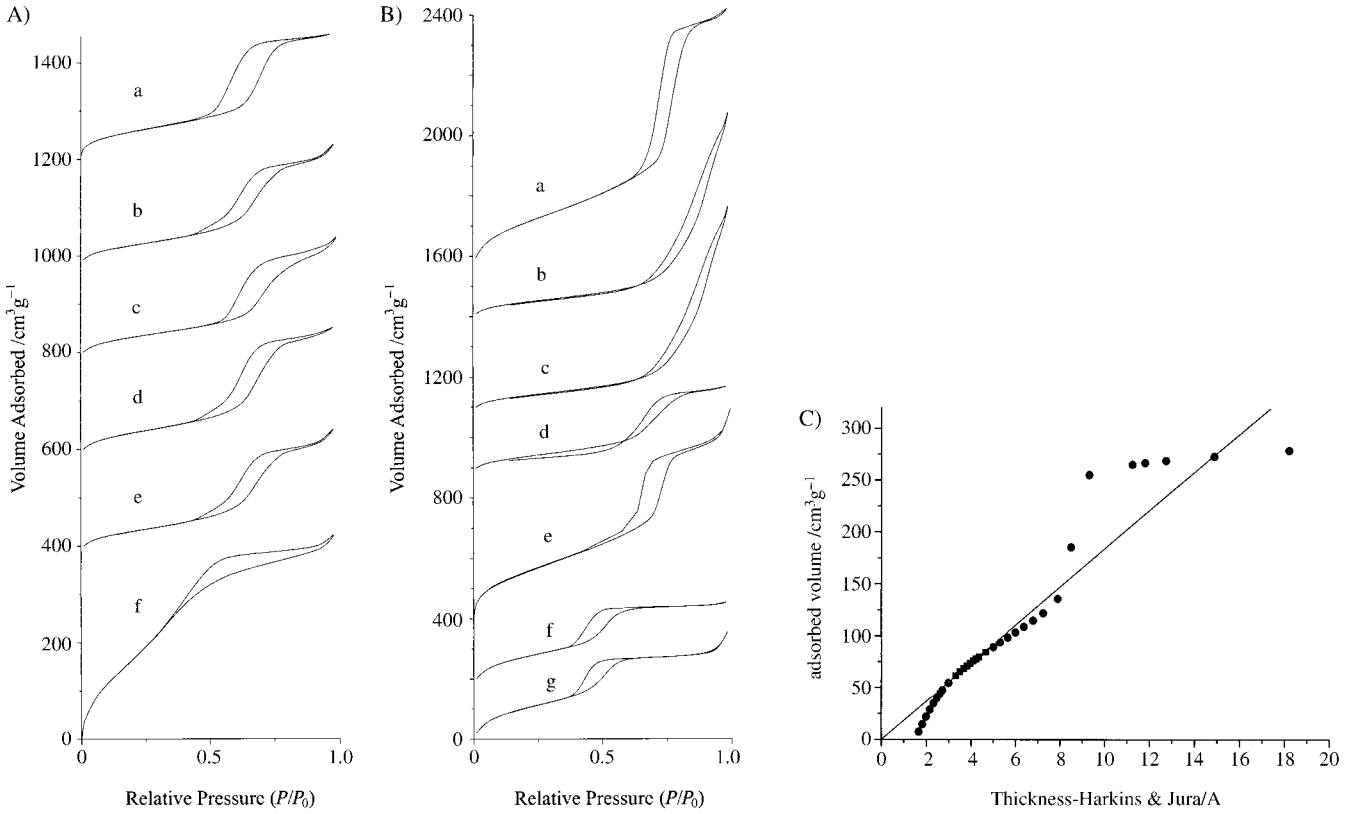

Figure 2. A) N_2 isotherms of **JLU-20** calcined at 650 °C (a), **JLU-20** calcined at 1000 °C (b), **JLU-20** treated in boiling water for 80 h (c), **JLU-20** compressed under 300 MPa for 10 min (d), **JLU-20** compressed under 740 MPa for 10 min (e), and the silica materials designated as **SFC-4**(190) synthesized at 190 °C using **FC-4** surfactant (f). The isotherms for a, b, c, d, and e are offset from 1200, 1000, 800, 600, and 400 $cm^3 g^{-1}$, respectively, for clarity. B) N_2 adsorption–desorption isotherms of **SBA-15** calcined at 500 °C (a), **SBA-15** calcined at 1000 °C (b), **SBA-15** treated in boiling water for 80 h (c), **SBA-15** compressed at 300 MPa for 10 min (d), **SBA-15**(B) calcined at 500 °C (e), **SBA-15**(B) compressed at 300 MPa for 10 min (f) and **SBA-15**(B) compressed at 740 MPa for 10 min (g). The isotherms for a, b, c, d, e, and f are offset from 1600, 1400, 1100, 900, 400, and 200 $cm^3 g^{-1}$, respectively, for clarity. C) N_2 adsorption isotherm *t*-plots of calcined **JLU-20**.

noteworthy that the pore-size distribution is very broad compared with those of **SBA-15** calcined at 500 °C. These results indicate that a large amount of the mesopores collapse under a pressure of 300 MPa. However, after the same pressure treatment (300 MPa), **SBA-15**(B) with thicker walls shows a better N_2 isotherm (Figure 2B-f) and higher surface area (677 $m^2 g^{-1}$, Table 1). These results confirm that **SBA-15** with thicker walls has better mechanical stability than conventional **SBA-15**, and is in good agreement with those reported in literature.[20] A further increase of pressure to 740 MPa yields a BET surface area and pore volume for **SBA-15**(B) of 559 $m^2 g^{-1}$ and 0.39 $cm^3 g^{-1}$, indicating that only 61 % of the surface area and 34 % of the pore volume are retained (Figure 2B-g). All of these results confirm that **JLU-20** has much better mechanical stability than **SBA-15** with both thin and thick mesoporous walls.

Figure 2A-f shows the N_2 isotherm of the sample synthesized at 180 °C by using the fluorocarbon surfactant **FC-4** in the absence of the hydrocarbon surfactant **P123**; the isotherm is not a IV-type isotherm. The BET surface area is 256 $m^2 g^{-1}$ with a pore-size distribution of 2.5 nm (Table 1). These results have demonstrated that the sample synthesized at higher temperature by using the fluorocarbon surfactant in the absence of a hydrocarbon surfactant is disordered. Therefore, surfactant mixtures of both fluorocarbon surfactant and hydrocarbon surfactant are necessary for the high-temperature synthesis of ordered mesoporous materials in our case.

It is worthy to note that calcined **JLU-20** has a relatively low surface area (300 $m^2 g^{-1}$) and pore volume (0.46 $cm^3 g^{-1}$) when compared with **SBA-15**. It has been reported that **SBA-15** has a specific surface area and pore volume which are far too large for a material with approximately uniform cylindrical (or hexagonal) pores, and that there might be a large number of micropores in the walls.[22] However, **JLU-20** strictly fulfils the fundamental relation between the structural parameters for materials with uniform pores of simple cylindrical geometry: $wSV^{-1} \approx 4$ (w, S, and V denote pore size, surface area and pore volume, respectively).[22] This suggests that, unlike **SBA-15**, **JLU-20** is almost free of micropores in the mesoporous walls. This is confirmed by N_2 adsorption isotherm *t*-plots (Figure 2C), which show that the micropore volume and micropore area are 0.005 $cm^3 g^{-1}$ and 20 $m^2 g^{-1}$, respectively. Considering the absence of micropores in the walls and the thicker walls with higher density, the relatively low values of surface area and pore volume in the case of **JLU-20** are reasonable.

Transmission electron microscopy (TEM): The image taken in the [100] direction (Figure 3A) of calcined **JLU-20** shows well-ordered hexagonal arrays of mesopores with 1D channels and further confirm that **JLU-20** has a 2D hexagonal (*p6mm*) mesostructure. From bright–dark contrast in the TEM image of the sample (Figure 3A), the mesopore size and wall thickness is estimated to be 6.0 nm and 5.8 nm, in a good agreement with the value determined from XRD.

Figure 3B shows the images taken in the [110] direction with 1D channels for a large area, which indicate that **JLU-20** exists as only one phase. This further confirms that **JLU-20** is really a pure phase as indicated by XRD results. Interestingly, **JLU-20** has continuous zigzag mesoporous channels that can be as long as 6 μm (Figure 3B), much longer than in conventional **SBA-15**.[4] Such continuous ultra-long channels have not been reported before. Additionally, we have also observed mesostructural patterns in these images such as "fingerprint-like" (Figure 3C), "Y-like" (Figure 3D), "fork-like" (Figure 3E) and "homocentric circle or helix tube" (Figure 3F). We suggest that these mesostructural patterns may result from the special properties of the fluorocarbon–hydrocarbon surfactant mixtures at high temperature and are currently under investigation in our laboratory. Moreover, unlike most ordered mesoporous materials that are extremely vulnerable to heating and electron radiation,[23] **JLU-20** is not damaged even under relatively strong current density for a long time (over 30 min). This is another indication that **JLU-20** possesses unusual stability.

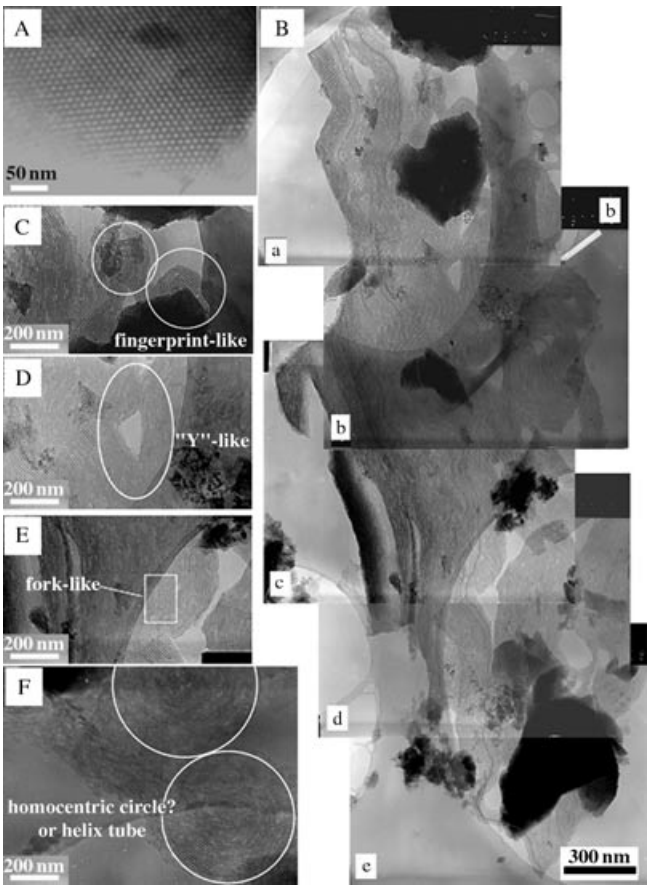

Figure 3. A) TEM image of calcined **JLU-20** taken in the [100] direction. B) TEM image of calcined **JLU-20** taken in the [110] direction. The ordered region is so large that fives photos (a–e) had to be taken. The five images are arranged in succession to completely show the continuous ultra-long channels, two of which are marked for clarity. C–F) Four TEM images of calcined **JLU-20** taken in the [110] direction.

^{29}Si high-resolution magic angle spinning nuclear resonance (HR MAS NMR) spectroscopy: Figure 4A shows a ^{29}Si NMR spectrum of as-synthesized **JLU-20**, providing direct evidence of the extent of silica condensation. In general, ordered mesoporous silica materials exhibit three bands cen-

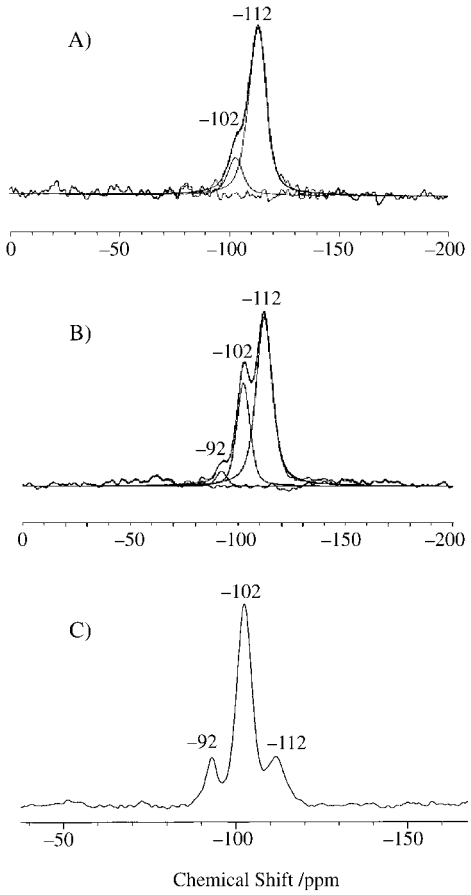

Figure 4. ^{29}Si HR MAS NMR spectra of as-synthesized A) **JLU-20**, B) **SBA-15**, and C) **SBA-15** (B).

tered at chemical shifts of $\delta = -92$, -102, and -112 ppm, which can be attributed to $Si(OSi)_x(OH)_{4-x}$ framework units, where $x = 2$ (Q^2), $x = 3$ (Q^3), and $x = 4$ (Q^4), respectively. Notably, as-synthesized **JLU-20** is primarily made up of fully condensed Q^4 silica units ($\delta = -112$ ppm). A small contribution comes from incompletely cross-linked Q^3 ($\delta = -102$ ppm), as deduced from the very high Q^4/Q^3 ratio of 6.5:1, whereas no Q^2 units were observed (Figure 4A). In contrast, **SBA-15** and **SBA-15** (B) have typical peaks corresponding to Q^2, Q^3, and Q^4 silica species, with ratios of $Q^4/(Q^3+Q^2)$ 1.9:1 and 0.23:1 (Figure 4B, Figure 4C), respectively, suggesting the presence of a large number of terminal hydroxy groups in the walls. This difference implies that high temperatures favor the formation of mesoporous materials with more completely cross-linked frameworks, which have higher thermal, hydrothermal, and mechanical stability. As shown in Figure 1A, though treated in boiling water for 80 h or in 100% steam at 800°C for 2 h or under pressure of 740 MPa for 10 min, **JLU-20** still maintains its 2D hexagonal (*p6mm*) mesostructure. To our knowledge, **JLU-20** has the highest degree of silica condensation among all kinds of mesoporous silica materials, except for the vesicle-like MSU-G that has a similarly high degree of SiO_4 cross-linking.[5] However, MSU-G has a poorly ordered mesostructure (analogous to the L_α-L_3 intermediate structure) and no textural properties, such as surface area and pore volume, of the hydrothermally treated MSU-G was shown to justify its high hydrothermal stability.

Thermogravimetry analysis (TGA): Figure 5a shows the TGA curve of as-synthesized **JLU-20**, exhibiting a total weight loss of about 25%, which occurs in three steps: 5%

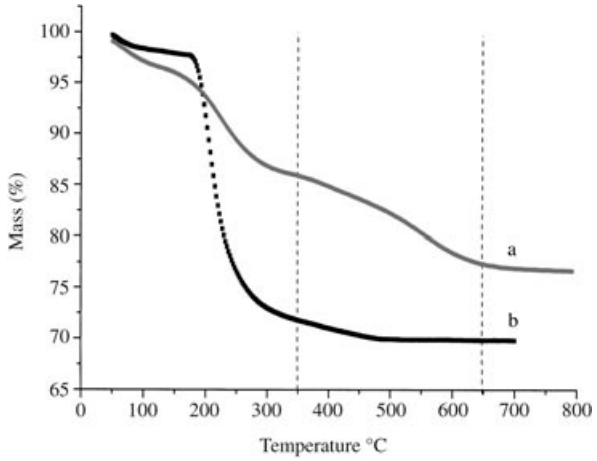

Figure 5. Thermogravimetry (TGA) curve of as-synthesized **JLU-20** (a) and **SBA-15** (b).

weight loss at 50–150°C due to water desorption, 10% weight loss at 150–350°C due to **P123** decomposition, and 10% weight loss at 350–650°C due to **FC-4** decomposition. In contrast, the TGA curve of as-synthesized **SBA-15** (Figure 5b) shows that the total weight loss is about 38% and mainly occurs at 150–400°C due to decomposition of the polymeric surfactant **P123**.[24,25] These results suggest that there are two kinds of surfactants in nearly equal quantities in the as-synthesized **JLU-20**, and is further confirmed by the results of elemental analysis. For example, the content of nitrogen in the as-synthesised sample is close to 0.5%. We calculate, according to the ratio of nitrogen and fluorocarbon surfactant, the content of fluorocarbon surfactant in as-synthesized **JLU-20** to be near 12%, which is similar to the 10% weight loss found from the TGA results. It is possible that, during the synthesis of **JLU-20**, **FC-4** and **P123** are entangled to form mixed micelles rather than forming separate micelles in the aqueous solution.

Surface tension measurements: Figure 6 shows the surface tension of aqueous solutions of **FC-4**, **P123**, and their mixture (1:2 weight ratio) versus the logarithm of concentration at 20.0°C, respectively. Generally, the critical micelle concentration (CMC) is obtained as the break point of the curve. **FC-4** shows a CMC value at 7.080 gL^{-1}, and **P123** exhibits a CMC value at 44.667 gL^{-1}. Importantly, the aqueous mixture of **FC-4** and **P123** has only one CMC with a lower value at 3.020 gL^{-1}, suggesting there is only one surfactant micelle in the aqueous solution.[26] This confirms that **P123** and **FC-4** are entangled with each other to form a mixed micelle rather than independent micelles of **P123** and **FC-4** in the aqueous solution.[26–28] Possibly, when a silica source is

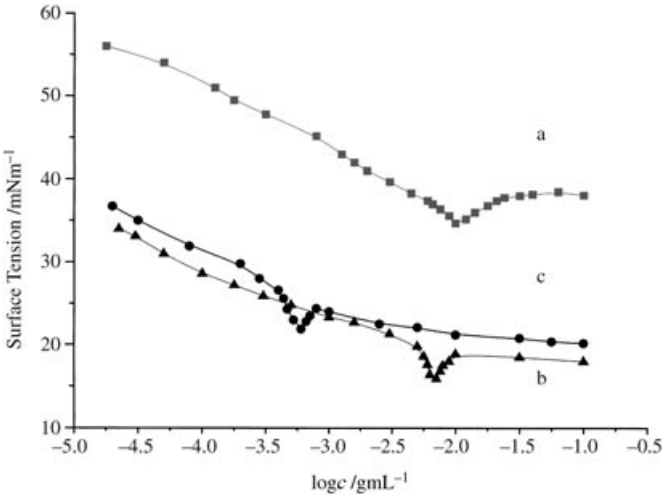

Figure 6. Equilibrium surface tension (mNm^{-1}) of **FC-4** (a), **P123** (b), and their mixture (**FC-4**+**P123**) (c) in aqueous solutions as a function of the logarithm of bulk concentration at 20 °C.

added into the synthesis system, hydrolyzed Si species can interact with the mixed micelles of **P123** and **FC-4** through $S^0(H^+)X^-I^+$ and $S^+X^-I^+$ routes, respectively, to form the mesostructure.[11–12] Although a part of **P123** surfactant may decompose at high temperature (>180 °C), **FC-4** successfully preserves the mesostructure from collapse because of its special stability towards high temperatures. It is noted that disordered mesoporous silica with a BET surface area of 256 $m^2 g^{-1}$ (Figure 2A-f) is obtained if only **FC-4** (without **P123**) is used for the synthesis. This may be attributed to the fact that the fluorocarbon surfactant tends to assemble into small-sized micelles, instead of periodic long-range ordered micelles, due to the rigidity and strong hydrophobicity of the fluorocarbon chain.[13]

The complete silica condensation and high thermal, hydrothermal, and mechanical stabilities of **JLU-20** should be attributed directly to the high synthesis temperature rather than other reasons, such as the presence of fluorocarbon surfactant. If **JLU-20** is prepared at 100 °C instead of at 190 °C, it shows no difference in both structural properties (such as surface area, pore volume, Q^4/Q^3 ratio, Table 1) and stabilities with conventional **SBA-15**, although **FC-4** is used. However, the use of the fluorocarbon surfactant allows full condensation by a high-temperature synthesis route.

Ordered cubic mesoporous silica materials (JLU-21)

Cubic mesoporous materials, for example **SBA-16**[21] and MCM-48,[2] have the advantage of 3D structures that may lead to better diffusion and transport of molecules than 2D hexagonal mesophases, such as MCM-41 and **SBA-15**, when used as catalysts or catalyst supports. However, most of the academic and industrial interest is concentrated on the 2D hexagonal mesophases, and there are only a very limited number of studies on the hydrothermal stability of 3D cubic mesoporous silica materials, possibly due to the difficulty of their synthesis. In our case, when the fluorocarbon surfactant (**FC-4**) is mixed with a triblock copolymer surfactant (**F127**) and this mixture used as a template, cubic *Im*3*m* mesoporous silica materials, designated **JLU-21**, are successfully synthesized in strongly acidic media at various temperatures (100 °C, 140 °C, and 180 °C). The obtained samples are denoted as **JLU-21**$_{100}$, **JLU-21**$_{140}$ and **JLU-21**$_{180}$, respectively. For comparison, a cubic **SBA-16** *(Im*3*m)* is prepared with only **F127** as a template at relatively low temperature (80 °C).

XRD investigations: Figures 7a–c show XRD patterns of calcined **JLU-21** synthesized at 100, 140, and 180 °C, respectively. Notably, calcined **JLU-21**$_{100}$ and **JLU-21**$_{140}$ clearly exhibit two peaks that could be indexed as the (110) and (200) reflections associated with a highly ordered cubic mesophase, in agreement with the HR TEM images (see Figure 9). However, when the synthesis temperature is increased to 180 °C, **JLU-21**$_{180}$ shows only one peak associated with the (110) reflection, with weaker intensity, indicating a relatively poor mesostructural ordering. The lattice constants (unit-cell parameters) of these samples can be calculated from the *d* values of the main (110) peaks and are

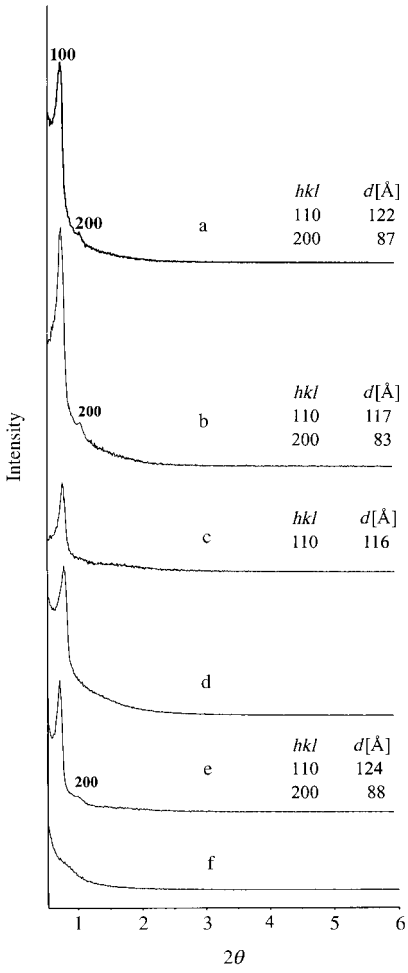

Figure 7. XRD patterns of calcined **JLU-21**$_{100}$ (a), **JLU-21**$_{140}$ (b), **JLU-21**$_{180}$ (c), **JLU-21**$_{140}$ treated in boiling water for 100 h (d), calcined **SBA-16** (e), and calcined **SBA-16** treated in boiling water for 100 h (f).

found to decrease with increased synthesis temperature. The lattice constants of **SBA-16** prepared at 80 °C, **JLU-21**$_{100}$, **JLU-21**$_{140}$, and **JLU-21**$_{180}$ are 17.5, 17.2, 16.5, and 16.4 nm, respectively (Figure 7e, Figure 7a–c). This may be attributed to the fact that the higher synthesis temperatures are favorable for the condensation of siliceous species on the pore walls, leading to further shrinkage of the unit cell.

Interestingly, upon the hydrothermal treatment in boiling water for 100 h, the XRD pattern of **JLU-21**$_{140}$ shows no significant changes in the *d* spacing and intensity, indicating the successful retention of its mesostructural symmetry (Figure 7d). In contrast, **SBA-16** prepared at 80 °C loses most of its mesostructure during the same treatment, as indicated by the XRD result (Figure 7f). These results indicate that **JLU-21**$_{140}$ has much better hydrothermal stability than **SBA-16**.

N_2 isotherms: Figure 8 shows nitrogen isotherms for calcined and hydrothermally treated **JLU-21**$_{140}$ and **SBA-16** samples. The isotherms of **JLU-21**$_{140}$ (Figure 8A-a) and **SBA-16** (Figure 8A-d) have a broad hysteresis loop, characteristic of materials with uniform, cagelike mesopores with entrances (or "windows") much narrower than the diameter of the cage itself.[29–31] According to the previous studies,[31–32] when the nitrogen capillary evaporation at 77 K from a cage-like pore is delayed to the lower pressure limit of hysteresis, just as in the case of **SBA-16**, the pore entrance diameter has to be below 5 nm. The mesoporous material **JLU-21**$_{140}$ exhibits slightly different adsorption properties from the samples prepared at low temperature. The capillary evaporation of **JLU-21**$_{140}$ begins at relative pressures much higher than the lower limit of adsorption–desorption hysteresis, suggesting the existence of pore entrances larger than 5 nm.[32] Similar results, that is, that an increase in the synthesis temperature can enlarge the entrances of the cages, have been found in previous studies.[32–33] Notably, although the broadness of the relative pressure range for the capillary evaporation suggests a broad distribution of entrance sizes in **JLU-21**$_{140}$, the pore sizes of the cages are still very uniform as indicated by the steep capillary condensation in the adsorption branch of the isotherm.

After hydrothermal treatment in boiling water for 100 h, there is only a 6% decrease in the BET surface area (from 556 $m^2 g^{-1}$ to 525 $m^2 g^{-1}$) for **JLU-21**, whereas it is 86% for **SBA-16** (from 852 $m^2 g^{-1}$ to 114 $m^2 g^{-1}$, Table 2). The mesopore volume of **JLU-21** increases during the treatment from 0.65 $cm^3 g^{-1}$ to 0.83 $cm^3 g^{-1}$, whereas that of **SBA-16** decreases dramatically from 0.74 $cm^3 g^{-1}$ to 0.25 $cm^3 g^{-1}$ (Table 2). In contrast, the same hydrothermal treatment for **SBA-16** results in complete loss of the typical isotherm for a cubic mesostructure (Figure 8A-e), indicating complete destruction of **SBA-16**. These results confirm the retention of structural integrity in the treated **JLU-21** and the better hydrothermal stability of **JLU-21** compared with that of **SBA-16**.

Interestingly, after the treatment in boiling water for 100 h, the broad hysteresis loop, which is characteristic of materials with cagelike mesopores with much narrower entrances, disappears in the isotherm of **JLU-21**. Instead, the treated **JLU-21** displays a classical H1-type isotherm with a narrow hysteresis loop, which is characteristic of materials with a channel-like pore structure (Figure 8A-b). This change may be attributed to the fact that the pore entrances in **JLU-21** has been enlarged during the hydrothermal treatment so that their sizes are almost as large as those of the interior diameter of the cages. The pore structure of **JLU-21**

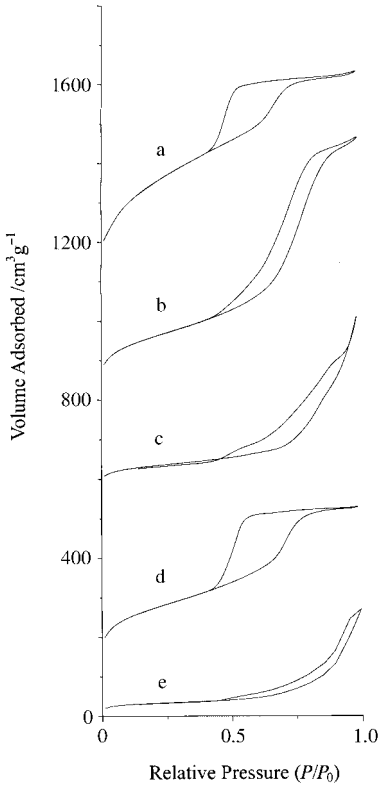

Figure 8. N_2 adsorption–desorption isotherms of calcined **JLU-21**$_{140}$ (a), calcined **JLU-21**$_{140}$ treated in boiling water for 100 h (b), calcined **JLU-21**$_{180}$ (c), calcined **SBA-16** (d), and calcined **SBA-16** treated in boiling water for 100 h (e). The isotherms for a, b, c, and d are offset from 1200, 900, 600, and 200 $cm^3 g^{-1}$, respectively, for clarity.

Table 2. Properties of **SBA-16** and **JLU-21**$_{140}$ before and after hydrothermal treatment in boiling water for 100 h.

Sample	Unit cell parameter [Å]	Pore cage diameter[a] [Å]	Mesopore volume [$cm^3 g^{-1}$][b]	BET surface area [$m^2 g^{-1}$]
SBA-16	175	82	0.74	852
treated[c]	—	—	0.25	114
SBA-16$_{140}$	159	—	0.31	232
JLU-21$_{140}$	165	78	0.65	556
treated	165	86	0.83	525
JLU-21$_{100}$	172	56	1.12	735
JLU-21$_{180}$	164	—	0.31	102

[a] Pore cage diameter is estimated by using BJH methods developed for cylindrical pores. There may be some underestimations because of the spherical pores of these samples.[22] Because **SBA-16** was rendered amorphous after the hydrothermal treatment, there are no unit-cell parameters and pore size for the treated **SBA-16** sample given in this table. [b] BJH adsorption cumulative pore volume of pores between 20 and 200 Å diameter. [c] Treated in boiling water for 100 h.

becomes more open, that is, without the original restrictions caused by narrow entrances. Additionally, the hydrothermal treatment also results in an increase in pore cage diameter (Table 2), which is indicated by the fact that the capillary condensation takes place at a higher relative pressure range.

Figure 8A-c shows the isotherm of **JLU-21**$_{180}$, which, due to its irregularity, indicates a relatively disordered mesostructure. This is consistent with the XRD result and shows that an excessively high temperature is not favorable for the retention of a well-ordered mesostructure. Notably, the 2D hexagonal **JLU-20** (*p*6*mm*) was successfully synthesized at the ultra-high temperature of 190 °C and its structure was still highly ordered.[15] In this case, however, the structural ordering of cubic **JLU-21** will be destroyed substantially if the synthesis temperature used is more than 140 °C, as shown by the results of XRD and N_2 adsorption investigations above. This may be explained by the structural difference between **JLU-20** and **JLU-21**. Unlike rodlike **JLU-20**, the structure of **JLU-21** is cagelike (spherical) with a much higher surface curvature and lower density of siliceous species on the walls. Therefore, further silica condensation associated with the high synthesis temperature has more influence on the structure of **JLU-21** and the retention of the uniform structure of **JLU-21** is more difficult at high temperatures.

TEM investigations: Figure 9 shows HR TEM images of large well-ordered areas of [100], [110], and [111] incidences

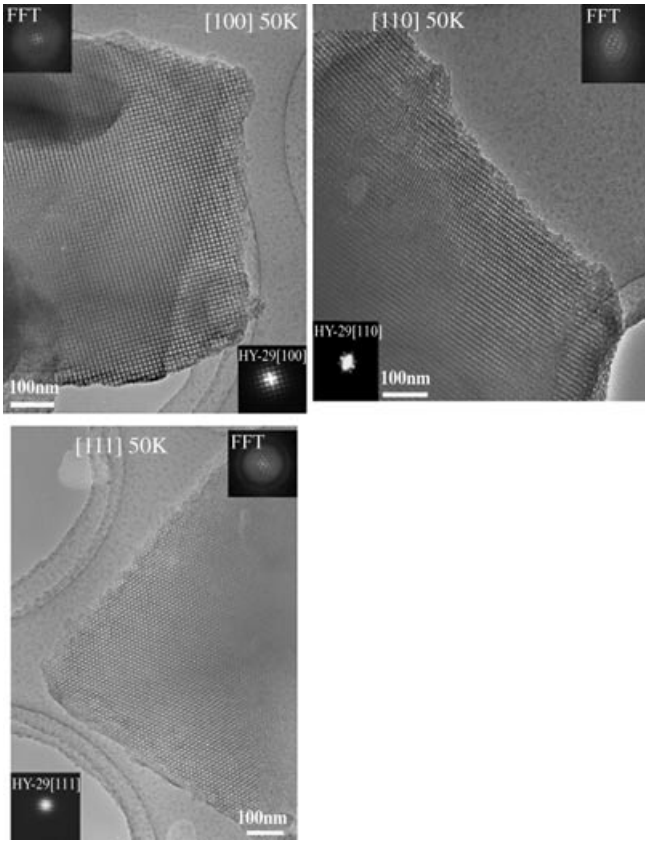

Figure 9. TEM images of [100], [110], and [110] incidence of the cubic **JLU-21**$_{140}$, as shown separately. Insets are the selected-area ED and FFT patterns of these images.

for calcined **JLU-21**$_{140}$. Clearly, the arrays of these uniform cages are highly ordered, demonstrating that **JLU-21**$_{140}$ has excellent structural ordering for a cubic space group (*Im*3*m*).

Figure 10 shows HR TEM images of calcined **JLU-21**$_{140}$ treated in boiling water for 100 h. In the TEM images of the treated **JLU-21**$_{140}$, large areas with uniform mesopore arrays

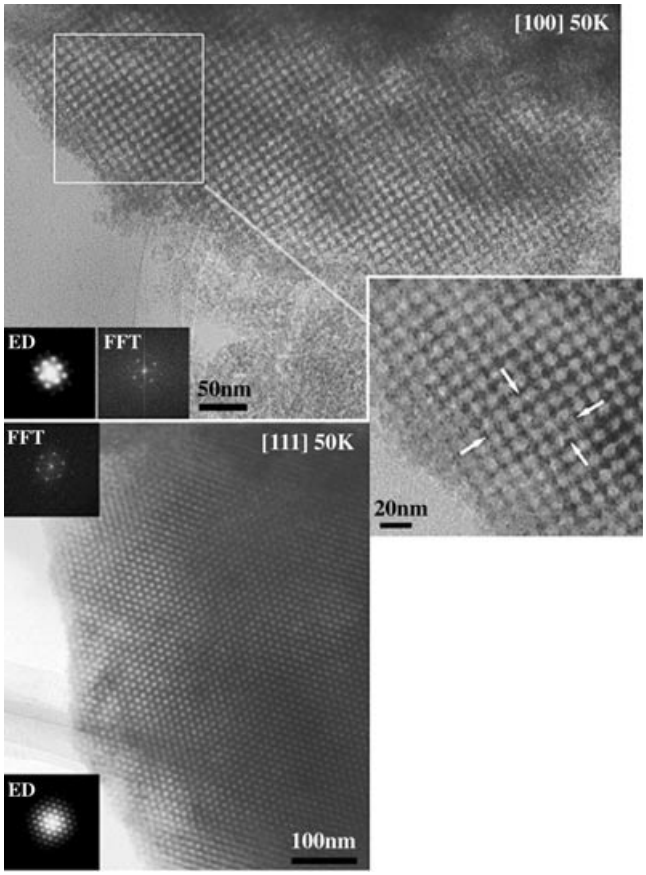

Figure 10. TEM images of **JLU-21**$_{140}$ treated hydrothermally in boiling water for 100 h. Insets are the corresponding ED and FFT patterns. Arrows indicate the enlarged pore entrances ("windows") that result in a highly open mesoporous structure.

belonging to different incidence are clearly observed, revealing a well-retained cubic mesostructure. In the high magnification image taken in the [100] direction, arrows indicate that the pore entrances have been substantially enlarged. Their size is close to the size of the cage pore itself, resulting in an open porous structure such as those of the channel-like samples. This is in good agreement with the conclusion drawn from the N_2 adsorption isotherm studies (Figure 8A-b). Evidently, the enlargement of the pore size by hydrothermal treatment has hardly any influence on the whole structure symmetry. The highly open, ordered, 3D pore system would facilitate diffusion and transport of molecules and should be helpful for a variety of potential applications of mesoporous silica materials.

^{29}Si HR MAS NMR spectroscopy: Figure 11 shows the ^{29}Si MAS NMR spectra of as-synthesized **SBA-16** and **JLU-21**,

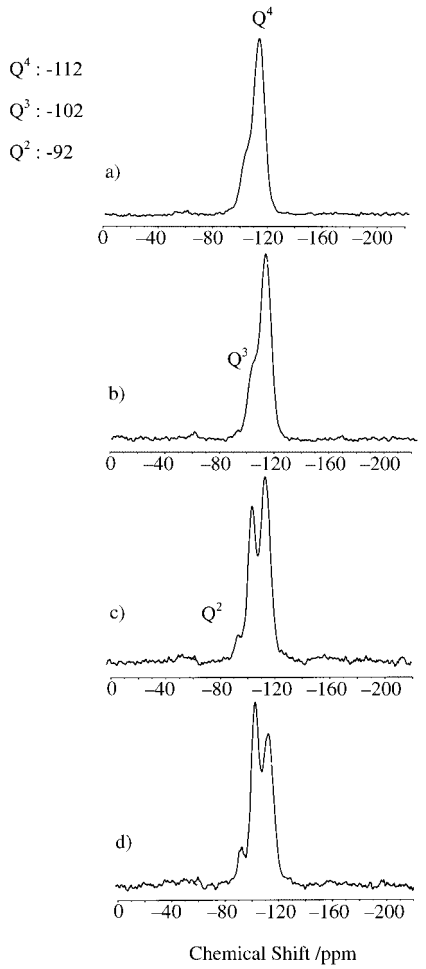

Figure 11. ^{29}Si NMR spectra of as-synthesized **JLU-21**$_{180}$ (a), **JLU-21**$_{140}$ (b), **JLU-21**$_{100}$ (c), and **SBA-16** (d).

which provide direct results for the different extent of silica condensation in these samples. In mesoporous silica materials, the most observed bands, centered at chemical shifts of $\delta = -112$, -102, and -92 ppm, can be attributed to $Si(OSi)_4$, $Si(OSi)_3OH$ and $Si(OSi)_2(OH)_2$ units, respectively. As observed in Figure 11, it is clear that the degree of silica condensation on the pore walls tends to increase with the synthesis temperature. For example, the proportion of fully condensed silica units (Q^4) in **SBA-16** is relatively low with a ratio of Q^4/Q^3+Q^2 at 0.8, indicating the presence of large amounts of terminal hydroxy groups in the walls. The Q^4/Q^3+Q^2 ratio of **JLU-21**$_{100}$ is 1.2, obviously higher than that of **SBA-16**. No Q^2 signals are observed in the case of **JLU-21**$_{140}$ and **JLU-21**$_{180}$. This indicates that they are primarily made up of fully condensed Q^4 silica units with a small contribution from incompletely cross-linked Q^3, as deduced from the very high Q^4/Q^3 ratio (5.4 and 7.1 for **JLU-21**$_{140}$ and **JLU-21**$_{180}$, respectively). These results indicate that relatively high synthesis temperatures are indeed favorable for promoting silica condensation on the pore walls.

TGA analyses: The thermogravimetry curve of as-synthesized **JLU-21** shows a total weight loss of 36 wt%. This also occurs in three steps, including water desorption (weight loss of 8 wt%), **F127** decomposition (weight loss of 13 wt%), and **FC-4** decomposition (weight loss of 15 wt%), just as discussed in the case of **JLU-20**. Moreover, we have estimated that the content of fluorocarbon surfactant in as-synthesised **JLU-21** is near 18%, according to the result of elemental analysis (the content of nitrogen in the as-synthesized sample is 0.6%). These results also confirm that **F127** and **FC-4** coexist in as-synthesized **JLU-21**. During the synthesis of **JLU-21**, **FC-4** and **F127** are possibly also entangled to form mixed micelles.

Surface tension measurements: Figure 12 shows the surface tension of aqueous solutions of **FC-4**, **F127**, and their mixture (at a 1:1 weight ratio) versus the logarithm of concentration at 20.0°C, respectively. Interestingly, the aqueous mixture of **FC-4** and **F127** also has only one CMC, indicating there is only one type of micelle in the aqueous mixture.[24] Furthermore, the CMC value of this mixture (3.020 gL^{-1}) is also less than that of **FC-4** (7.080 gL^{-1}) and **F127** (44.667 gL^{-1}). These results support the notion that **F127** and **FC-4** are entangled with each other to form a mixed micelle rather than independent micelles of **F127** and **FC-4** in the aqueous solution.[26–28] When a silica source is added to the synthesis system, hydrolyzed Si species can interact with the mixed micelle of **F127** and **FC-4** to form the mesostructure.[11–12] Notably, although **F127** may decompose partly at high temperature (>140°C) under hydrothermal conditions, **FC-4** successfully prevents the collapse of the fluorocarbon–hydrocarbon mixed micelles because of its special stability towards high temperatures.

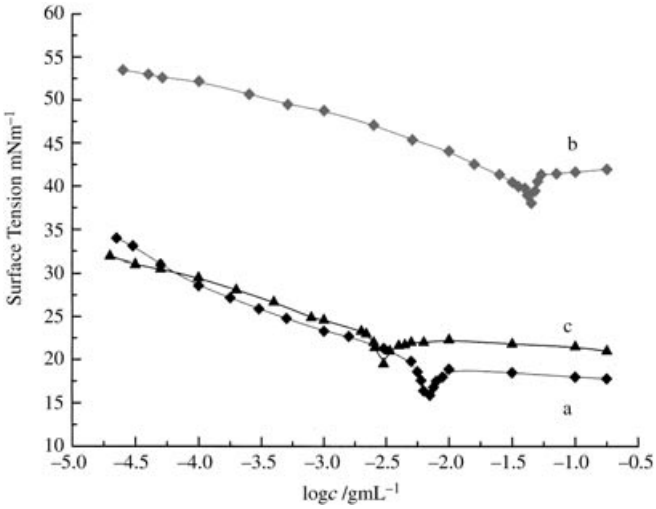

Figure 12. Equilibrium surface tension (mNm^{-1}) of **FC-4** (a), **F127** (b), and their mixture (**FC-4**+**F127**) (c) in aqueous solutions as a function of the logarithm of bulk concentration at 20°C.

The complete silica condensation and high hydrothermal stability of **JLU-21** should be directly attributed to the high temperature of the synthesis, just as discussed in the case of the stable hexagonal mesoporous silica **JLU-20**. We have tried to synthesize **SBA-16** using **F127** as template in the absence of **FC-4** at relatively high temperature (140°C), but

the obtained material shows a disordered mesostructure without uniform mesopores, as indicated by XRD and N_2 adsorption isotherm. This result demonstrates the indispensability of the fluorocarbon surfactant for the high-temperature synthesis of stable cubic mesoporous silica materials (**JLU-21**).

Conclusion

Mesoporous silica materials (**JLU-20**) with a highly ordered hexagonal mesostructure have been synthesized hydrothermally at high temperature (150–220 °C) using a fluorocarbon–hydrocarbon surfactant mixture as a template. The materials have fully condensed mesoporous walls, and exhibit extraordinarily high thermal, hydrothermal, and mechanical stability, which is superior to most other mesoporous materials. Furthermore, the concept of "high-temperature synthesis" is successfully extended to the preparation of 3D cubic mesoporous silica materials by the assistance of the fluorocarbon surfactant as a co-template. The obtained material **JLU-21** also has a well-ordered cubic *Im*3*m* mesostructure with fully condensed pore walls and shows unusually high hydrothermal stability.

Experimental Section

Synthesis of materials: Typical synthesis procedures for various mesoporous silica materials are as follows:

JLU-20: The fluorocarbon surfactant **FC-4** (1.2 g) and **P123** (0.4 g) were dissolved in H_2O (20 mL) and HCl (5 mL, 10 M), followed by the addition of tetraethyl orthosilicate (TEOS, 2.4 mL). After stirring at 40 °C for 20 h, the mixture was transferred into an autoclave for further condensation. The crystallization temperature was slowly increased to 190 °C over 10 h and maintained there for 30 h. The product was collected by filtration, dried in air and calcined at 650 °C for 5 h to remove the surfactant template. In comparison, the silica sample **JLU-20**(100), was hydrothermally synthesized at 100 °C using the same mixed micelle composition of **FC-4** and **P123** in a strongly acidic medium. The silica samples named **SFC-4**(100) and **SFC-4**(190) were hydrothermally synthesized at 100 °C and 190 °C using **FC-4** as a template in the absence of **P123** in strongly acidic media.

JLU-21: The fluorocarbon surfactant **FC-4** (0.5 g) and **F127** (0.5 g) were dissolved in H_2O (20 mL) and HCl (5 mL, 10 M), followed by the addition of tetraethyl orthosilicate (TEOS, 2.0 mL). After stirring at room temperature for 20 h, the mixture was transferred into an autoclave for further condensation at different temperatures (100, 140, or 180 °C) for 24 h. The product was collected by filtration, dried in air and calcined at 650 °C for 5 h to remove the surfactant template. The products are denoted **JLU-21**$_{100}$, **JLU-21**$_{140}$, and **JLU-21**$_{180}$, respectively.

SBA-15 and **SBA-15**(B): The materials **SBA-15** and **SBA-15**(B) with thicker walls were synthesized at 100 °C and 37 °C for two days, respectively, according to the procedure published by Zhao, Stucky et al.[21] In comparison, the silica sample named **SBA-15**(190), was hydrothermally synthesized at 190 °C using **P123** as a template, in the absence of **FC-4**, in a strongly acidic medium.

SBA-16: The material **SBA-16** was synthesized at 80 °C for 24 h, according to the procedure published by Zhao, Stucky et al.[21] In comparison, the silica sample **SBA-16**(140), was synthesized at 140 °C using **F127** as a template in a strongly acidic medium.

Stability tests: The hydrothermal stability of samples was tested by treatment in boiling water (0.5 L of water per gram of solid) for 80–100 h or in 100 % steam at 800 °C for 2 h. Thermal stability of samples was tested by calcination in air at 1000 °C for 4 h. To test the mechanical stability, calcined samples were compressed in a steel die of 13 mm diameter for 10 min using a hand-operated press. The three different external pressures applied (0, 300, and 740 MPa) were calculated from the external force applied and the diameter of the die.

Characterization: X-ray diffraction patterns (XRD) were obtained with a Siemens D5005 diffractometer using $Cu_{K\alpha}$ radiation. Transmission electron microscopy experiments were performed on a JEM-300CX electron microscope (JEOL, Japan) with an acceleration voltage of 300 kV. The nitrogen adsorption and desorption isotherms were measured at the temperature of liquid nitrogen using a Micromeritics ASAP 2020 M system. The samples were degassed for 10 h at 300 °C before the measurements. ^{29}Si NMR spectra were recorded on a Varian Infinity plus 400 spectrometer. The samples were fitted in a 7 mm ZrO_2 rotor, spinning at 8 kHz. A Perkin-Elmer TGA 7 unit was used to carry out the thermogravimetric analysis (TGA) in air at a heating rate of 20 °C min^{-1}. Surface tensions of aqueous surfactant solutions at various concentrations were measured with a ZZHY-220 tensiometer. All measurements were carried out at 20.0 ± 0.5 °C, and each experiment was repeated several times until reproducibility was achieved. The critical micelle concentration (CMC) values of **FC-4**, **P123**, **F127**, the mixture of **FC-4** with **P123** (1:1 weight ratio of 1:1), and the mixture of **FC-4** with **F127** (1:1 weight ratio) were determined by the sharp break point in the surface tension against the logarithm of concentration curves.

Acknowledgement

This work is supported by the NSFC, CNPC, the National High Technology Research and Development Program of China (863 Program) and State Basic Research Project (973 Program).

[1] A. Corma, *Chem. Rev.* **1997**, *97*, 2373.
[2] C. T. Kresge, M. E. Leonowicz, W. J. Roth, J. C. Vartuli, J. S. Beck, *Nature* **1992**, *352*, 710.
[3] R. Mokaya, *J. Phys. Chem. B* **1999**, *103*, 10204.
[4] D. Zhao, J. Feng, Q. Huo, N. Melosh, G. H. Fredrickson, B. F. Chmelka, G. D. Stucky, *Science* **1998**, *279*, 548.
[5] S. S. Kim, W. Zhang, T. J. Pinnavaia, *Science* **1998**, *282*, 1032.
[6] R. Ryoo, J. M. Kim, C. H. Shin, *J. Phys. Chem.* **1996**, *100*, 17718.
[7] a) R. Mokaya, *Chem. Commun.* **1998**, 1839; b) R. Mokaya, *Angew. Chem.* **1999**, *111*, 3079; *Angew. Chem. Int. Ed.* **1999**, *38*, 2930; c) R. Mokaya, *Chem. Commun.* **2001**, 633.
[8] a) Y. Liu, W. Zhang, T. J. Pinnavaia, *J. Am. Chem. Soc.* **2000**, *122*, 8791; b) Y. Liu, W. Zhang, T. J. Pinnavaia, *Angew. Chem.* **2001**, *113*, 1295; *Angew. Chem. Int. Ed.* **2001**, *40*, 1255.
[9] a) Z. Zhang, Y. Han, L. Zhu, R. Wang, Y. Yu, S. Qiu, D. Zhao, F.-S. Xiao, *Angew. Chem.* **2001**, *113*, 1298–1302; *Angew. Chem. Int. Ed.* **2001**, *40*, 1258–1262; b) Y. Han, S. Wu, Y. Sun, D. Li, F.-S. Xiao, *Chem. Mater.* **2002**, *14*, 1144; c) Y. Han, F.-S. Xiao, S. Wu, Y. Sun, X.-J. Meng, D, Li, S. Lin, *J. Phys. Chem. B* **2001**, *105*, 7963.
[10] F.-S. Xiao, Y. Han, X.-J. Meng, Y. Yu, M. Yang, S. Wu, *J. Am. Chem. Soc.* **2002**, *124*, 888.
[11] T. Sun, J. Y. Ying, *Nature* **1997**, *389*, 704.
[12] J. S. Beck, J. C. Vartuli, G. J. Kennedy, C. T. Kresge, W. J. Roth, S. E. Schramm, *Chem. Mater.* **1994**, *6*, 1816.
[13] Y. Muto, K. Esumi, K. Meguro, R. Zana, *J. Colloid Interface Sci.* **1987**, *120*, 162.
[14] N. Funasaki, S. Hada, *J. Phys. Chem. B.* **1983**, *87*, 342.
[15] Y. Han, D.-F. Li, L. Zhao, J. Song, X. Yang, N. Li, Y. Di, C. Li, S. Wu, X. Xu, X. Meng, K. Lin, F.-S. Xiao, *Angew. Chem.* **2003**, *115*, 3765; *Angew. Chem. Int. Ed.* **2003**, *42*, 3633.
[16] M. Kruk, M. Jaroniec, *Chem. Mater.* **2000**, *12*, 1961.
[17] M. Kruk, M. Jaroniec, A. Sayari, *Chem. Mater.* **1999**, *11*, 492.
[18] B. P. Feuston, J. B. Higgins, *J. Phys. Chem. B* **1994**, *98*, 4459.
[19] P. Agren, M. Linden, J. B. Rosenholm, R. Schwarzenbacher, M. Kriechbaum, H. Amenitsch, P. Laggner, J. Blanchard, F. Schuth, *J. Phys. Chem. B* **1999**, *103*, 5943.
[20] M. Hartmann, A. Vinu, *Langmuir* **2002**, *18*, 8010.

[21] D. Zhao, Q. Huo, J. Feng, B. F. Chmelka, G. D. Stucky, *J. Am. Chem. Soc.* **1998**, *120*, 6024.
[22] R. Ryoo, C. H. Ko, M. Kruk, M. Antochshuk, M. Jaroniec, *J. Phys. Chem. B* **2000**, *104*, 11465.
[23] J. Liu, X. Zhang, Y. Han, F.-S. Xiao, *Chem. Mater.* **2002**, *14*, 2536.
[24] Q. Huo, D. I. Margolese, U. Ciesla, D. G. Demuth, P. Feng, T. E. Gier. P. Sieger, A. Firouzi, B. F. Chemlka, F. Schuth, G. D. Stucky, *Chem. Mater.* **1994**, *6*, 1176.
[25] C. Chen, H. Li, M. E. Davis, *Microporous Mater.* **1993**, *2*, 17.
[26] T. Suzuki, M. Ueno, K. Meguro, *J. Am. Oil Chem. Soc.* **1981**, *58*, 800.
[27] K. Yada, K. Tamori, K. Esumi, K. Meguno, *J. Colloid Interface Sci.* **1989**, *131*, 282.
[28] B. Y. Zhu, M. J. Rosen, *J. Colloid Interface Sci.* **1984**, *99*, 435.
[29] Y. Sakamoto, M. Kaneda, O. Terasaki, D. Zhao, J. -M. Kim, G. D. Stucky, H. J. Shin, R. Ryoo, *Nature* **2000**, *408*, 449.
[30] C. Yu, Y. Yu, D. Zhao, *Chem. Commun.* **2000**, 575.
[31] J. R. Matos, L. P. Mercuri, M. Kruk, M. Jaroniec, *Langmuir* **2002**, *18*, 884.
[32] J. R. Matos, M. Kruk, L. P. Mercuri, M. Jaroniec, L. Zhao, O. Terasaki, T. J. Pinnavaia, Y. Liu, *J. Am. Chem. Soc.* **2003**, *125*, 821.
[33] J. Fan, C. Yu, L. Wang, Y. Sakamoto, O. Terasaki, B. Tu, D. Zhao, in *Abstract of 3rd International Mesostructured Materials Symposium*, July 8–11, **2002**, PA-22, p. 72.

Received: July 27, 2004
Published online: October 14, 2004

